



OPEN

Abnormal drop in electrical resistivity with impurity doping of single-crystal Ag

SUBJECT AREAS:
ELECTRONIC PROPERTIES
AND MATERIALS
ELECTRONIC STRUCTUREJi Young Kim^{1*}, Min-Wook Oh^{2*}, Seunghun Lee^{3†}, Yong Chan Cho⁴, Jang-Hee Yoon⁵, Geun Woo Lee⁶, Chae-Ryong Cho¹, Chul Hong Park⁷ & Se-Young Jeong³Received
23 December 2013Accepted
5 June 2014Published
26 June 2014Correspondence and
requests for materials
should be addressed to
C.H.P. (cpark@pusan.
ac.kr) or S.-Y.J.
(syjeong@pusan.ac.kr)* These authors
contributed equally to
this work.† Current address: The
Institute of Basic
Science, Korea
University, Seoul, 136-
713, Republic of
Korea.

¹Department of Nano Fusion Technology, Pusan National University, Miryang, 627-706, Republic of Korea, ²Fundamental and Creativity Research Division, Korea Electrotechnology Research Institute, Changwon-si, 642-120, Republic of Korea, ³Department of Cogno-Mechatronics Engineering, Pusan National University, Miryang, 627-706, Republic of Korea, ⁴Crystal Bank Research Institute, Pusan National University, Miryang 627-706, Republic of Korea, ⁵Busan center, Korea Basic Science Institute, Busan, 618-230, Republic of Korea, ⁶Korea Research Institute of Standards and Science & Department of Science of Measurement, University of Science and Technology, Daejeon, 305-340, Republic of Korea, ⁷Department of Physics Education & RCDAMP, Pusan National University, Busan, 609-735, Republic of Korea.

Resistivity is an intrinsic feature that specifies the electrical properties of a material and depends on electron-phonon scattering near room temperature. Reducing the resistivity of a metal to its potentially lowest value requires eliminating grain boundaries and impurities, but to date few studies have focused on reducing the intrinsic resistivity of a pure metal itself. We could reduce the intrinsic resistivity of single-crystal Ag, which has an almost perfect structure, by impurity doping it with Cu. This paper presents our results: resistivity was reduced to 1.35 $\mu\Omega\cdot\text{cm}$ at room temperature after 3 mol% Cu-doping of single-crystal Ag. Various mechanisms were examined in an attempt to explain the abnormal behavior.

Metals are considered to be ideal materials for electronics, because of their superior electrical properties¹. Silver (Ag) is the best conductor at room temperature, with a resistivity of 1.59 $\mu\Omega\cdot\text{cm}$ at 293 K, which may be expressed as 108% according to the International Annealed Copper Standard (IACS). The high conductivity of metals, especially Ag, makes them ideal for many industrial power applications, in which excellent printing, thermal, electrical, wire-bonding, and soldering properties are a prerequisite^{2–6}. Many researchers have recently tried to develop advanced metal materials with greater power consumption and higher efficiency for the aerospace and medical industries^{7–14}. Although superconductors are ideal for this purpose, their low critical transition temperature (T_c) remains a limiting factor for practical applications. Thus, considerable research has focused on developing new materials with higher conductivity at room temperature (RT)^{15–17}.

The resistivity of a material increases as a result of imperfections, such as defects, impurities, grain boundaries, and dislocations¹⁸. The resistivity of single-crystal copper (Cu) (1.52 $\mu\Omega\cdot\text{cm}$ at 293 K, 113.4% IACS) is 12% lower than that of polycrystalline Cu, which is even lower than that of polycrystalline Ag, due to the elimination of grain boundaries via the crystal growth process¹⁹. Another approach to reducing resistivity involves the simultaneous application of heat and pressure after crystal growth, which can enhance the crystallinity of the metal and thereby significantly reduce resistivity (e.g., for Cu, a 14% reduction in resistivity: 1.472 $\mu\Omega\cdot\text{cm}$ at 293 K, 117.1% IACS)²⁰.

The resistivity of alloys is generally higher than that of pure metals, and increases with impurity contamination^{21,22}. However, we report here a surprising decrease in resistivity by addition of a certain amount of Cu impurity to single-crystal Ag, which is an ideal conductor at room temperature. Copper wire of high purity has a conductivity of slightly over 103% IACS, which is close to the value expected for Cu with no impurities. Here, we report an uncharacteristic increase in conductivity, to 127% IACS, as a result of Cu impurities in single-crystal Ag.

Single-crystal Cu, single-crystal Ag, and $\text{Ag}_{1-x}\text{Cu}_x$ mixed crystals ($x = 1, 2, 3, 5,$ and 10 mol%) were grown using the Czochralski method (all equipment was supported by Crystal Bank at Pusan National University). Figure 1 shows an example of an $\text{Ag}_{0.95}\text{Cu}_{0.05}$ mixed crystal. These pole-figure images, obtained using X-ray diffraction (XRD) (Fig. 1b, c), confirm the crystallinity of the $\text{Ag}_{1-x}\text{Cu}_x$ crystals (additional pole-figure images of other $\text{Ag}_{1-x}\text{Cu}_x$ mixed crystals are provided in Supplementary Information Fig. 1). The crystal quality of the Ag-Cu mixed crystals was slightly lower than that of pure single-crystal Cu and Ag, but the mixed crystals exhibited well-defined growth along the (111) direction, up to a Cu-alloy ratio of 10 mol%, and most of the copper atoms were substituted into Ag sites. Samples for resistivity measurements were prepared by wire cutting using electrical discharge machining (EDM), as shown in the inset to Figure 1e.

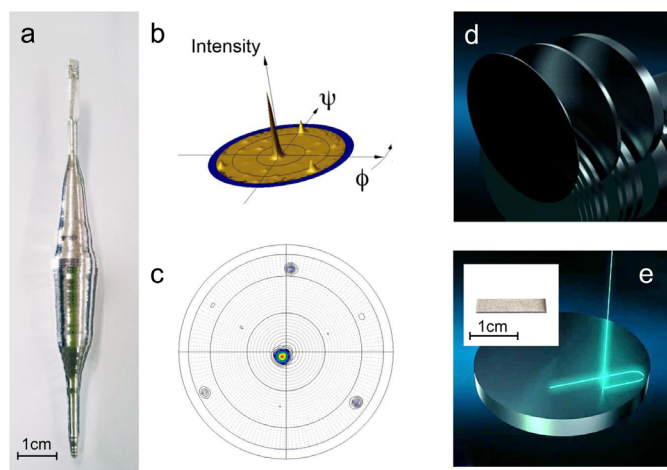


Figure 1 | Grown Ag-Cu mixed crystal and its fabrication.

(a): Photograph of the 5% Cu-doped Ag mixed crystal, grown using the Czochralski method. (b) and (c): 2.5D and 2D pole-figure images obtained from the metal mixed crystal. (d) and (e): Sample-cutting image using a wire electrical discharge machine (EDM). Inset to (e): Sample for electrical resistivity measurements using the four-point probe method. All photographs were taken by S.Y.J. and the co-authors.

Compositional analysis was carried out using glow-discharge spectrometry (GDS). We confirmed that the Cu atoms were homogeneously distributed with the intended amount. Concentrations of impurities other than Cu were negligible, compared with that of Cu. The distribution of unintentional impurities, other than Ag and Cu, are shown in the Supplementary Information section (Fig. S2 and Table 1).

Figure 2a shows the electrical resistivity for various Ag/Cu materials at room temperature. The resistivity of metals is known to increase with the addition of impurities, and is also higher in mixed crystals or alloys than in pure crystalline materials.

However, we observed, unexpectedly, that resistivity decreased after doping with small amounts of Cu, up to 3 mol%. The lowest resistivity was obtained in the 3 mol% Cu (◆)-doped Ag mixed crystal; its resistivity was $1.35 \mu\Omega\cdot\text{cm}$, which is 9.4% lower than that of single-crystal Ag (●) ($1.49 \mu\Omega\cdot\text{cm}$). The resistivities near 3 mol% ($\pm 0.1, 0.2\%$) of Cu were slightly higher than that of 3 mol% (inset, Fig. 2(a)). The resistivity of greater than 5 mol% Cu-doped Ag was slightly higher than that of single-crystal Ag. Resistivity increased slightly at greater than 5 mol% Cu-doped Ag. The resistivities of the 5 mol% Cu (◀)- and 10 mol% Cu (▶)-doped Ag crystals were 1.51 and $1.66 \mu\Omega\cdot\text{cm}$, respectively, slightly higher than that of pure single-crystal Ag. This is the first report of this uncharacteristic drop in resistivity due to Cu doping.

In contrast, the alloy (*not* grown as a single crystal) exhibited an increase in resistivity as a result of Cu addition. The alloy was

prepared by furnace cooling from the melt state. The 3 mol% Cu-doped alloy (◇) had a resistivity of $1.76 \mu\Omega\cdot\text{cm}$, a 23.3% increase over that of the $\text{Ag}_{0.97}\text{Cu}_{0.03}$ mixed crystal.

The different consequences of Cu doping in the alloy and the single crystal may be attributable to the short-range order of Cu in the mixed crystal and the reduced number of grain boundaries. The liquid cooling rate is much slower for crystal growth, resulting in an increase in the probability of short-range ordering.

Figure 2b shows the temperature dependences of the electrical resistivity of polycrystalline $\text{Ag}_{0.97}\text{Cu}_{0.03}$ alloy, single-crystal Ag, and the $\text{Ag}_{0.97}\text{Cu}_{0.03}$ mixed crystal (See Figure S3 for the other samples). The lowered resistivity at the low temperature of 10 K reflects the fact that the doped Cu impurities did not contribute to electron-impurity scattering.

To understand the change in resistivity after the addition of Cu in the Ag single crystal, we first examined Matthiessen's experimental findings^{24,25}. According to Matthiessen's rule, the electrical resistivity of an impure metal can be separated into two contributions, given as:

$$\rho(c, T) = \rho_0(c) + \rho_i(T) \quad (1)$$

where ρ_0 is the temperature-independent residual resistivity, caused mainly by electron-impurity (*el-imp*) and electron-defect (*el-def*) scattering, and is dependent on the impurity concentration c , and ρ_i is the temperature-dependent intrinsic resistivity, determined mainly by electron-phonon (*el-ph*) scattering²⁶. For a ρ_0 of the binary solid-solution system, and considering Nordheim's rule, given as $\rho_0 \propto c(1-c)$, in which c is the mole fraction of Cu, the increased ρ for $>5\%$ Cu-doped mixed crystals can be attributed to the enlarged *el-imp* scattering. However, the change in ρ_i must be considered in understanding the drop in ρ in the $<5\%$ Cu-doped mixed crystals. The intrinsic resistivity ρ_i can be approximated by the Bloch-Grüneisen equation:

$$\rho(T) = \alpha_{el-ph} \left(\frac{T}{\Theta_D}\right)^5 \int_0^{\frac{\omega_p}{T}} \frac{x^5}{(e^x - 1)(1 - e^{-x})} dx \quad (2)$$

where Θ_D is the Debye temperature, x is a variable ranging from 0 to Θ_D/T , and the constant α_{el-ph} is proportional to $\lambda_{tr}\omega_D/\omega_p^2$, where λ_{tr} is the electron-phonon coupling constant, and ω_D and ω_p are the Debye and plasma frequencies, respectively^{18,27}. This equation is favored for metal elements, such as a monovalent metals with a spherical Fermi surface²⁸. The equation is composed of three parts: an electronic term (ω_p), a phonon-related term (Θ_D, ω_D), and an electron-phonon coupling term (λ_{tr}).

First, we consider the electronic term. The value of ω_p is known to be determined solely by the carrier concentration n and the effective mass of electrons m^* ($\omega_p^2 \propto n/m^*$). Thus, the electronic contribution toward the electrical resistivity can be understood based on the electronic structure. The electrical resistivity (ρ) can be described by the Boltzmann transport equation, given as:

Table 1 | Optimized lattice parameters (a_0), bulk modulus (B), estimated Debye temperature (Θ_D), and electron-phonon coupling constant (λ_{tr}) for Ag, Cu, and the mixed crystal

	a_0 [Å]	B [GPa]	Θ_D [K]	λ_{tr}
Ag	4.165	88.6	201.8	0.121 0.12 ³¹
Cu	3.637	136.2	327.1	0.135 0.116 ³⁰ 0.13 ³¹ 0.14 ³²
Cu-cu dimer.	4.150	90.6	140.0	0.109
Cu-Cu separated	4.150	90.7	203.0	0.108

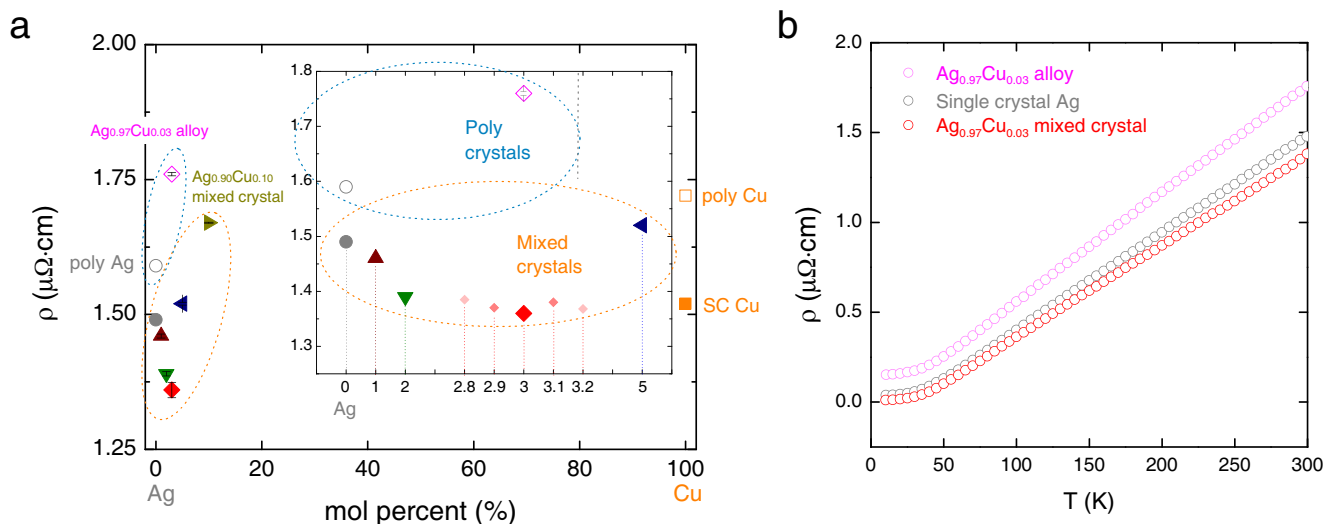


Figure 2 | Electrical resistivity of crystals. (a): Electrical resistivities of pure single-crystal Ag, Ag-Cu mixed crystals, and polycrystalline $\text{Ag}_{0.97}\text{Cu}_{0.03}$ alloy, measured at 300 K, and polycrystalline Cu, single-crystal Cu, and polycrystalline Ag, measured at 293 K^{19,23}. (b): Temperature dependences of electrical resistivity of the polycrystalline $\text{Ag}_{0.97}\text{Cu}_{0.03}$ alloy, single-crystal Ag, and $\text{Ag}_{0.97}\text{Cu}_{0.03}$ mixed crystal.

$$\rho(\varepsilon) = \left[\frac{e^2}{N\Omega} \int d\varepsilon \left(-\frac{\partial f_0}{\partial \varepsilon} \right) \sum_{n,k} \tau_{n,k} \vec{v}_{n,k} \vec{v}_{n,k} \delta(\varepsilon - \varepsilon_{n,k}) \right]^{-1} \quad (3)$$

where e is the charge of the carrier, N is the number of k -points used in the calculations, Ω is the volume of a unit cell, f_0 is the equilibrium Fermi-Dirac distribution function, $\tau_{n,k}$ is the relaxation time, $\vec{v}_{n,k}$ denotes the group velocity, $\varepsilon_{n,k}$ stands for the band energy, and δ is the delta function²⁹. The subscripts n and k represent the band index and crystal momentum in the case of a crystal solid, respectively. $\vec{v}_{n,k}$ can be derived from the band structure using the following relationship:

$$\vec{v}_{n,k} = \frac{1}{\hbar} \frac{\partial \varepsilon_{n,k}}{\partial \mathbf{k}} \quad (4)$$

Thus, the value of ρ can be obtained from the electronic structure and the exact value of τ . In principle, the value of τ is dependent on the band energy $\varepsilon_{n,k}$ and temperature; however, we assumed the value was constant to estimate how changing the electronic structure of the mixed crystal affected the electrical resistivity. Moreover, we assumed a rigid band approximation. The Fermi level was obtained from the total number of electrons in the unit cells, and was used to calculate ρ .

The electrical resistivities were estimated from the electronic structures of the Ag, Cu, and mixed crystal, in which electronic structures of the supercell model were used for all systems. The model with a composition of 3.125 mol% Cu was used to estimate the electrical resistivity of 3 mol% Cu mixed crystals. The configuration of the Cu atoms was considered to investigate the effects of Cu-Cu interaction on the electronic structure and the electrical resistivity. We simulated the two extreme systems: i) the dimerized state of two Cu atoms (distance between Cu-Cu ($d_{\text{Cu-Cu}}$) = 2.824 Å), and ii) the furthest Cu-Cu separated system within a supercell ($d_{\text{Cu-Cu}}$ = 8.300 Å). The dimer state was more stable, by 12 meV, than the latter case (Fig. S4 in SI). The density of states of the two systems is compared in Figure S5 (in SI) and shows a clear difference between the systems, indicating that there is an effect of ordering on electronic structure. The estimated electrical resistivity from the electronic structure of the dimer system at room temperature can be lower, by ~1%, than that of Ag (Fig. 3). The same value of τ was used for all systems. These results indicated that clustering of Cu can lead to a reduction in the electronic resistivity, compared with pure Ag. The

amount of reduction of ρ from the electronic structure was smaller than that of the experimental value in Figure 2.

The lowered electrical resistivity in the mixed crystal cannot be fully understood by the change in the electronic structure alone. Thus, in addition to the electronic term, the phonon-related term, Θ_D and ω_D , was considered to be a cause of the drop in ρ . From Eq. (2) and the equation $\omega_D = k_B \Theta_D / h$, where k_B is Boltzmann's constant and h is Planck's constant, we can see that the Debye temperature Θ_D has a significant influence on ρ . Θ_D was calculated from the phonon density of states (Table 1). The Θ_D value for the mixed crystal of the Cu-separated system was slightly greater than that of Ag, while that of the Cu-dimer system was much smaller. These results indicate that the phonon properties are also greatly dependent on Cu-ordering.

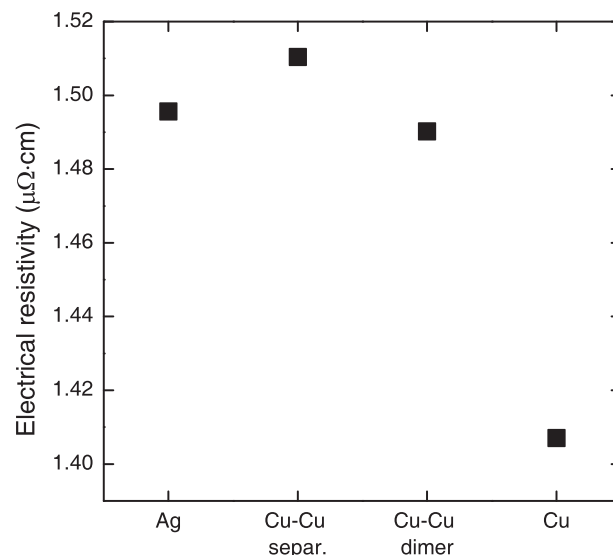


Figure 3 | Calculated electrical resistivity of Ag, Cu, Cu-Cu dimerized, and Cu-Cu separated systems. Electronic structures of the supercell were used to evaluate the properties. All values were obtained with the Boltzmann transport equation with a constant value of relaxation time of 3.4×10^{-14} s, chosen to fit the experimental resistivity of Ag.



It is known that λ_{tr} is independent of the temperature and can be obtained from the relationship between Θ_D , and τ when the temperature is greater than $0.7 \Theta_D^{33,34}$, given in Eq. (5):

$$\frac{\hbar}{\tau} = \frac{2\pi\lambda_{tr}k_B T}{F_{th}}, \quad (5)$$

where $F_{th} \cong (1 - \frac{0.038\Theta_D^2}{T^2})^{-1}$.

The value of τ must be known to evaluate λ_{tr} . In this study, the value of τ was estimated by comparing the experimental ρ with that obtained using Eq.(3). The evaluated values of λ_{tr} with τ and Θ_D are shown in Table 1. The estimated values of Ag and Cu were consistent with values in the literature. The value of λ_{tr} for the mixed crystal was lower than that of Ag. The reduced values were mainly due to the increased relaxation time, and the effect of the Debye temperature was limited. The relaxation time for coupling (or scattering) of the electrons to an acoustic phonon is dependent on the deformation potential, the density of materials, and the mean longitudinal sound velocity^{35,36}. We determined that the estimated sound velocity from phonon dispersion and the measured density did not lead to an increase in the relaxation time in the mixed crystal. Thus, the reduced scattering (i.e., increased relaxation time) was attributed mainly to the reduction in the deformation potential with Cu addition. On the other hand, the addition of Cu decreased the density, resulting in a reduction in the relaxation time. Thus, as the Cu amount increased, the change in the deformation potential had less influence. Due to tradeoff between these two effects, a minimum was observed in the resistivity of the mixed crystal at ~ 3 mol% Cu.

In addition to these intrinsic mechanisms, vacancy formation, an extrinsic effect, may also contribute to the low resistivity value. Our calculations indicated that the formation of a vacancy can be significantly suppressed in the presence of Cu within Ag. We estimated the formation energy of a vacancy through the total energy calculations of a cubic supercell having 32 atoms. The formation energy of a vacancy in Ag was estimated to be 0.74 eV, and it indicates that the concentration of vacancies can be quite high, $\sim 6.56 \times 10^{19} \text{ cm}^{-3}$ at growth temperature of 900°C. An interesting finding is that when one Ag is replaced by Cu, the formation energy of a vacancy increases greatly, and is estimated to be 1.19 eV for the vacancy located at the nearest site of Cu and 1.13 eV for the vacancy separated from Cu. This indicates that a small addition of Cu into Ag can reduce the concentration of vacancies significantly. Because the vacancy should be a strong scattering center, this suppression may explain the reduction in the resistivity by Cu addition. The formation of other Cu-related defective states due to the low solubility limit of Cu may lead to an increase in resistivity, as the concentration of Cu exceeds 3 mol%.

In summary, we observed an uncharacteristic drop in the resistivity of single-crystal Ag grown using the Czochralski method as a result of adding a small amount of Cu impurity (up to 3 mol%). We found that the change in the electronic structure, through Cu-Cu dimerization, benefits the reduction in the electrical resistivity, resulting in the resistivity of Cu-added Ag being lower than that of pure Ag. However, this electronic contribution alone is not sufficient to explain the significant drop in resistivity. Thus, we suggest that the reduced scattering may be due to the reduction in the deformation potential with Cu addition. From an extrinsic viewpoint, the suppression of vacancy formation in the presence of Cu within Ag may result in a reduction in resistivity due to the reduction in the concentration of vacancies, which behave as strong scattering centers.

Methods

Single-crystal Cu and Ag, and the $\text{Ag}_{1-x}\text{Cu}_x$ mixed crystals ($x = 1, 2, 3, 5$, and 10 mol%) were grown using the Czochralski method. To prevent oxidation during crystal growth, the growth process was conducted in an Ar gas (99.999%) atmosphere.

All samples were prepared carefully using the wire-EDM process from an ingot of mixed crystals^{19,20,37}. The crystal quality of the $\text{Ag}_{1-x}\text{Cu}_x$ mixed crystals was investigated by pole figure measurement using high-resolution XRD (PANalytical X'pert

PRO MRD). Radio frequency GDS (JY 10000 RF, KBSI-PA314, Korea Basic Science Institute, Busan Center) was used for compositional analyses of $\text{Ag}_{1-x}\text{Cu}_x$ mixed crystals and to identify any unintentional impurities.

Electrical resistivity and temperature were measured using the four-point probe method and a physical property measurement system (PPMS, Quantum Design, USA). We kept the contact area constant using gold-coated pogo pins to minimize the error caused by contact resistance. We used the reversal method, in which the voltages for current flow in one direction and the same current flow in the reverse direction are measured to reduce additional voltage due to thermoelectric effects. The reverse method gave us reliable data by eliminating the temperature difference between the two readings. We used a source meter (Keithley 2425-C) as the current source and a nanovoltmeter (Keithley 2182A) to measure drops in voltage.

The conventional unit cell of Ag and Cu can be described as face-centered cubic (FCC). For the electronic structure calculation, a primitive cell containing one atom was used for Ag and Cu. To describe the 3 mol% Cu-doped crystal, we constructed a $4 \times 4 \times 4$ supercell, and substituted two Cu atoms for Ag, representing 3.125 mol% Cu. All possible configurations were considered and the difference in the total energy is shown in Figure S4 (in SI). The electronic structure and structural optimization were carried out using the Vienna ab-initio simulation package (VASP)^{38,39}. Projector augmented-wave pseudopotentials were used⁴⁰. The exchange and correlation were treated within the generalized gradient approximation (PBE-GGA)⁴¹. The Brillouin zones (BZs) of the unit cell were represented by the gamma-centered Monkhorst-Pack scheme⁴². The BZs were sampled by at least $23 \times 23 \times 23$ and $5 \times 5 \times 5$ k-point meshes for the primitive unit cell and supercell, using the Methfessel-Paxton scheme with a smearing width of 0.1 eV⁴³. The plane wave-cutoff energy was greater than 400 eV for all calculations. The structures were fully relaxed using a quasi-Newton algorithm, until the force on each atom was within $10^{-5} \text{ eV \AA}^{-1}$. Electrical resistivity was estimated using the Boltzmann transport equation, implemented in the BoltzTraP code⁴⁴, assuming a rigid band approximation and constant relaxation time. The values of the k-point mesh were varied to investigate the convergence of the electrical resistivity and an intercept value at $1/(k\text{-point mesh}) = 0$ from an extrapolation was chosen. The largest value used in the extrapolation for the supercell was $35 \times 35 \times 35$.

Phonon calculations were performed using the supercell approach. Force constants were obtained using the framework of the density-functional perturbation theory (DFPT), implemented in VASP code, and phonon frequencies were calculated from the force constants using PHONOPY code⁴⁵. For comparison, the phonon frequencies were also calculated using the direct Parlinski-Li-Kawazoe method, with a finite displacement (FD) of 0.01 Å⁴⁶. The difference between the DFPT and FD methods was negligible. Supercells containing $4 \times 4 \times 4$ primitive cells (64 atoms) were used to calculate the phonon properties. We carried out the DFPT calculations using at least $5 \times 5 \times 5$ k-point grid meshes for BZ integration.

- Lu, K. The Future of Metals. *Science* **328**, 319–320 (2010).
- Wu, W., Brongersma, S. H., Van Hove, M. & Maex, K. Influence of surface and grain-boundary scattering on the resistivity of copper in reduced dimensions. *Appl. Phys. Lett.* **84**, 2838–2840 (2004).
- Park, M. W. *et al.* Highly stretchable electric circuits from a composite material of silver nanoparticles and elastomeric fibres. *Nature Nanotech.* **7**, 803–809 (2012).
- Lu, L., Shen, Y., Chen, X., Qian, L. & Lu, K. Ultrahigh Strength and High Electrical Conductivity in Copper. *Science* **304**, 422–426 (2004).
- Sakai, Y. & Schneider-Muntau, H.-J. Ultra-high strength, high conductivity Cu-Ag alloy wires. *Acta Mater.* **45**, 1017–1023 (1997).
- Wang, P. J., Kim, J. S. & Lee, C. C. Direct Silver to Copper Bonding Process. *J. Electron. Packag.* **130**, 045001-1-4 (2008).
- Lu, K., Lu, L. & Suresh, S. Strengthening Materials by Engineering Coherent Internal Boundaries at the Nanoscale. *Science* **324**, 349–352 (2009).
- Wang, Y., Chen, M., Zhou, F. & Ma, E. High tensile ductility in a nanostructured metal. *Nature* **419**, 912–915 (2002).
- Luechinger, N. A., Athanassiou, E. K. & Stark, W. J. Graphene-stabilized copper nanoparticles as an air-stable substitute for silver and gold in low-cost ink-jet printable electronics. *Nanotechnology* **19**, 445201 (2008).
- Lobodzinski, S. S. & Laks, M. New material for implantable cardiac leads. *J. Electrocardiology.* **42**, 566–573 (2009).
- Castro-Dettmer, Z., Simmons, M. & Persad, C. Obtainable Microstructures in Electrical Conductors Made of a Copper-Silver Alloy. *IEEE Transactions on Magnetics.* **39**, 323–326 (2003).
- Hansen, R. C. Superconducting Antennas. *IEEE Aerospace and Electronic Syst.* **26**, 345–355 (1990).
- Aricò, A. S., Bruce, P., Scrosati, B., Tarascon, J.-M. & van Schalkwijk, W. Nanostructured materials for advanced energy conversion and storage devices. *Nature Mater.* **4**, 366–377 (2005).
- Lee, J. *et al.* Very long Ag nanowire synthesis and its application in a highly transparent, conductive and flexible metal electrode touch panel. *Nanoscale* **4**, 6408–6414 (2012).
- Bird, M. D. Resistive magnet technology for hybrid inserts. *Supercond. Sci. Technol.* **17**, R19–R33 (2004).
- Müller, K. A. & Bednorz, J. G. The Discovery of a Class of High-Temperature Superconductors. *Science* **237**, 1133–1139 (1987).
- Grant, P. M. High-temperature superconductivity: The great quantum conundrum. *Nature* **476**, 37–39 (2011).



18. Ziman, J. M. *Electrons and Phonons* (Clarendon Press, Oxford, 1960).
19. Cho, Y. C. *et al.* Copper Better than Silver: Electrical Resistivity of the Grain-Free Single-Crystal Copper Wire. *Cryst. Growth Des.* **10**, 2780–2784 (2010).
20. Ajmal, M. *et al.* Fabrication of the best conductor from single-crystal copper and the contribution of grain boundaries to the Debye temperature. *Cryst. Eng. Comm.* **14**, 1463–1467 (2012).
21. Callister, W. D. Jr. *Materials Science and Engineering: An Introduction* (Wiley, New York, 2000).
22. Rossiter, P. L. *The electrical resistivity of metals and alloys* (Cambridge, 1991).
23. Stratton, S. W. *Circular Bureau of Standards* (No. 31, Appendix V. 1914).
24. Matthiessen, A. Ueber die elektrische Leitungsfähigkeit der Legierungen. *Ann. Phys. Chem.* **186**, 190–221 (1860).
25. Matthiessen, A. & Vogt, C. Ueber die elektrische Leitungsfähigkeit von Thallium und Eisen und über den Einfluss der Temperatur auf dieselbe. *Ann. Phys. Chem.* **194**, 431–444 (1864).
26. Ho, C. Y. *et al.* Electrical Resistivity of Ten Selected Binary Alloy Systems. *J. Phys. Chem. Ref. Data* **12**, 183–322 (1983).
27. Bid, A., Bora, A. & Raychaudhuri, A. K. Temperature dependence of the resistance of metallic nanowires of diameter ≥ 15 nm: Applicability of Bloch–Grüneisen theorem. *Phys. Rev. B* **74**, 035426-1-8 (2006).
28. Matula, R. A. Electrical Resistivity of Copper, Gold, Palladium, and Silver. *J. Phys. Chem. Ref. Data* **8**, 1147 (1979).
29. Oh, M. W., Wee, D. M., Park, S. D., Kim, B. S. & Lee, H. W. Electronic structure and thermoelectric transport properties of AgTlTe: First-principles calculations. *Phys. Rev. B* **77**, 165119-1-6 (2008).
30. Allen, P. B. *et al.* dc transport in metals. *Phys. Rev. B* **34**, 4331–4333 (1986).
31. Allen, P. B. Empirical electron-phonon λ values from resistivity of cubic metallic elements. *Phys. Rev. B* **36**, 2920–2923 (1987).
32. Savrasov, S. Y. & Savrasov, D. Y. Electron-phonon interactions and related physical properties of metals from linear-response theory. *Phys. Rev. B* **54**, 16487–16501 (1996).
33. Allen, P. B., Pickett, W. E. & Krakauer, H. Band-theory analysis of anisotropic transport in La₂CuO₄-based superconductors. *Phys. Rev. B* **36**, 3926–3929 (1987).
34. Mehta, R. J. *et al.* Seebeck and Figure of Merit Enhancement in Nanostructured Antimony Telluride by Antisite Defect Suppression through Sulfur Doping. *Nano Lett.* **12**, 4523–4529 (2012).
35. Oh, M. W., Gu, J. J., Inui, H., Oh, M. H. & Wee, D. M. Evaluation of anisotropic thermoelectric power of ReSi_{1.75}. *Physica B* **389**, 367–371 (2007).
36. Nag, B. R. *Electron Transport in Compound Semiconductors* (Springer, Berlin, 1980).
37. Cha, S.-Y. *et al.* Improving the precision of Hall effect measurements using a single-crystal copper probe. *Rev. Sci. Instrum.* **83**, 013901-1-5 (2012).
38. Kresse, G. & Furthmüller, J. Efficient iterative schemes for ab initio total-energy calculations using a plane-wave basis set. *Phys. Rev. B* **54**, 11169–11186 (1996).
39. Kresse, G. & Furthmüller, J. Efficiency of ab-initio total energy calculations for metals and semiconductors using a plane-wave basis set. *Comput. Mater. Sci.* **6**, 15–50 (1996).
40. Blöchl, P. E. Projector augmented-wave method. *Phys. Rev. B* **50**, 17953–17979 (1994).
41. Perdew, J. P., Burke, K. & Ernzerhof, M. Generalized Gradient Approximation Made Simple. *Phys. Rev. Lett.* **77**, 3865–3868 (1996).
42. Monkhorst, H. J. & Pack, J. D. Special points for Brillouin-zone integrations. *Phys. Rev. B* **13**, 5188–5192 (1976).
43. Methfessel, M. & Paxton, A. T. High-precision sampling for Brillouin-zone integration in metals. *Phys. Rev. B* **40**, 3616–3621 (1989).
44. Madsen, G. K. H. & Singh, D. J. BoltzTraP. A code for calculating band-structure dependent quantities. *Comput. Phys. Commun.* **175**, 67–71 (2006).
45. Togo, A., Oba, F. & Tanaka, I. First-principles calculations of the ferroelastic transition between rutile-type and CaCl₂-type SiO₂ at high pressures. *Phys. Rev. B* **78**, 134106-1-9 (2008).
46. Parlinski, K., Li, Z. Q. & Kawazoe, Y. First-Principles Determination of the Soft Mode in Cubic ZrO₂. *Phys. Rev. Lett.* **78**, 4063–4066 (1997).

Acknowledgments

This research was supported by the Converging Research Center Program through the Ministry of Science, ICT and Future Planning, Korea (MSIP) (2013K000310) and by the KERI Primary research program of MSIP/ISTK (No. 14-12-N0101-19). C.H.Park acknowledges the support by Basic Science Research Program through the National Research Foundation of Korea(NRF) funded by the Ministry of Education(No. 2013R1A1A2065742).

Author contributions

J.Y.K. performed crystal growth and measurements. M.W.O. and C.H.P. carried out theoretical work and data analyses. S.L. designed the experiments and performed data analysis and interpretation. Y.C.C., J.H.Y., G.W.L. and C.R.C. assisted with sample characterisation and contributed to measurement discussions. C.H.P. and S.Y.J. were responsible for project planning and guided the work. S.Y.J., M.W.O. and C.H.P. wrote the manuscript with help from the co-authors. All authors discussed the results and reviewed the manuscript.

Additional information

Supplementary information accompanies this paper at <http://www.nature.com/scientificreports>

Competing financial interests: The authors declare no competing financial interests.

How to cite this article: Kim, J.Y. *et al.* Abnormal drop in electrical resistivity with impurity doping of single-crystal Ag. *Sci. Rep.* **4**, 5450; DOI:10.1038/srep05450 (2014).



This work is licensed under a Creative Commons Attribution-NonCommercial-ShareAlike 4.0 International License. The images or other third party material in this article are included in the article's Creative Commons license, unless indicated otherwise in the credit line; if the material is not included under the Creative Commons license, users will need to obtain permission from the license holder in order to reproduce the material. To view a copy of this license, visit <http://creativecommons.org/licenses/by-nc-sa/4.0/>

Supplementary Information

Abnormal drop in electrical resistivity with impurity doping of single-crystal Ag

Ji Young Kim^{1[+]}, Min-Wook Oh^{2[+]}, Seunghun Lee^{3[-]}, Yong Chan Cho⁴, Jang-Hee Yoon⁵, Geun Woo Lee⁶, Chae-Ryong Cho¹, Chul Hong Park^{7*}, and Se-Young Jeong^{3*}

¹Department of Nano Fusion Technology, Pusan National University, Miryang, 627-706, Republic of Korea

²Fundamental and Creativity Research Division, Korea Electrotechnology Research Institute, Changwon-si, 641-120, Republic of Korea

³Department of Cogno-Mechatronics Engineering, Pusan National University, Miryang, 627-706, Republic of Korea

E-mail: syjeong@pusan.ac.kr

⁴Crystal Bank Research Institute, Pusan National University, Miryang 627-706, Republic of Korea

⁵Busan center, Korea Basic Science Institute, Busan, 618-230, Republic of Korea

⁶Korea Research Institute of Standards and Science & Department of Science of Measurement, University of Science and Technology, Daejeon, 305-340, Republic of Korea

⁷Department of Physics Education & RCDAMP, Pusan National University, Busan, 609-735, Republic of Korea

E-mail: cpark@pusan.ac.kr

[+] These authors contributed equally to this work.

[*] These authors contributed equally to this work as corresponding authors.

[-] Current address: The Institute of Basic Science, Korea University, Seoul, 136-713, Republic of Korea

Contents of Supplementary Information:

Figures S1-S5

Table S1

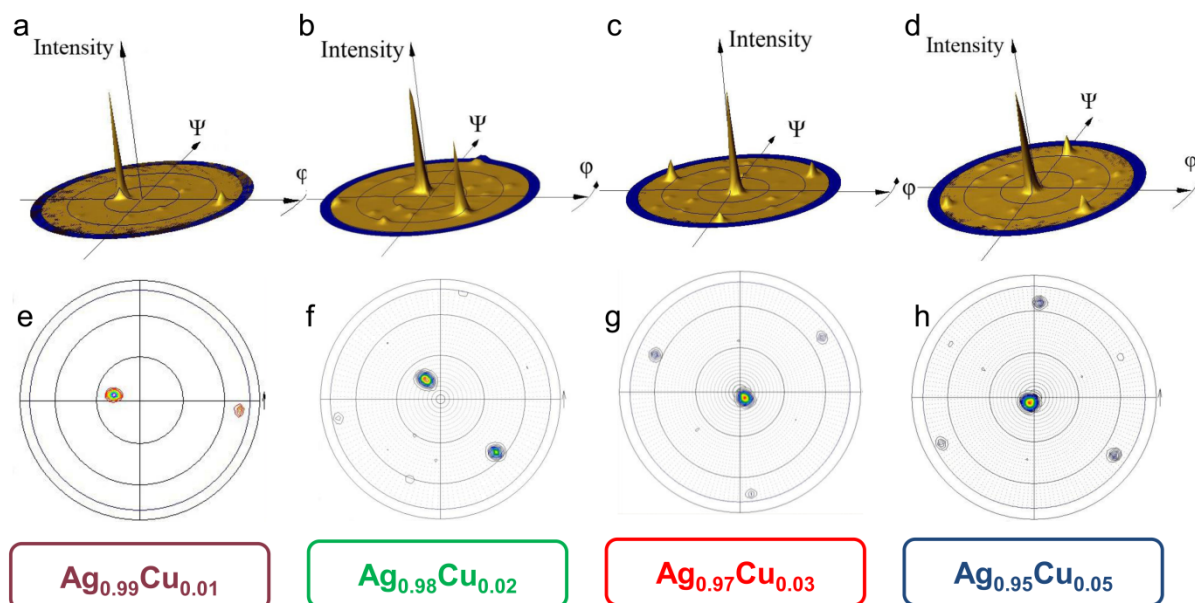


Figure S1. a–d: 2.5D XRD plots and e–h: 2D XRD plots of the (111) plane of the Ag–Cu mixed crystals $\text{Ag}_{0.99}\text{Cu}_{0.01}$, $\text{Ag}_{0.98}\text{Cu}_{0.02}$, $\text{Ag}_{0.97}\text{Cu}_{0.03}$, and $\text{Ag}_{0.95}\text{Cu}_{0.05}$.

Figure S1 shows the X-ray diffraction (XRD) plots of the (111) plane of the Ag–Cu mixed crystals, with Cu molar fractions in the range of 1–5%, demonstrating that the samples were single crystals. The mixed crystals were grown to exhibit features in the [111] direction, with the main peak slightly off-center. The presence of other smaller peaks suggests the presence of differently oriented domains or twin domains, which typically appear following a cutting process applied to soft metals.

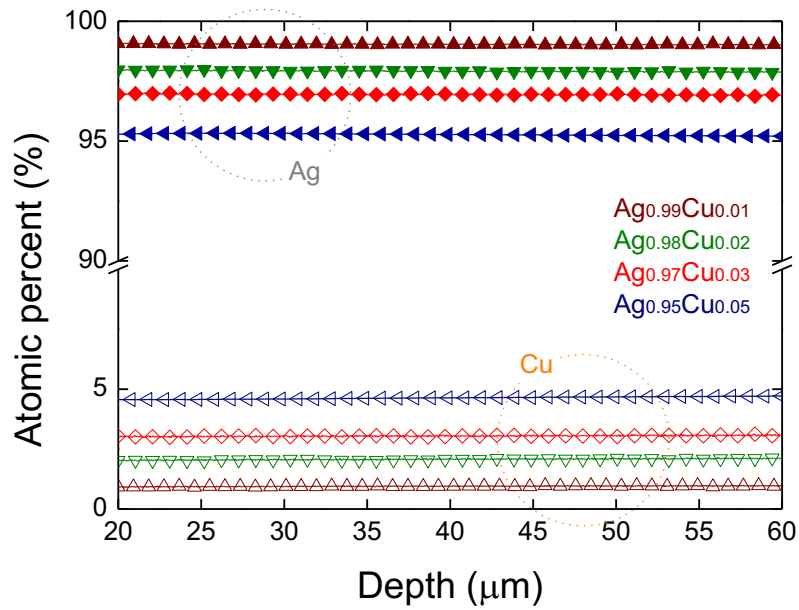


Figure S2. GDS depth profile elemental analyses of the Ag–Cu mixed crystals.

Figure S2 shows the atomic composition of the mixed crystals measured using glow discharge spectrometry (GDS). The measurement was carried out following etching, to remove surface impurities which may have been introduced during wire electrical discharge machining (EDM) cutting. Additional impurities (i.e., other than Ag and Cu) are listed in Table S1 for the $\text{Ag}_{0.97}\text{Cu}_{0.03}$ sample. The unintentional impurity levels in the $\text{Ag}_{0.99}\text{Cu}_{0.01}$, $\text{Ag}_{0.98}\text{Cu}_{0.02}$, and $\text{Ag}_{0.95}\text{Cu}_{0.05}$ samples were also similar.

Table S1. Atomic composition of unintentional impurities in $\text{Ag}_{0.97}\text{Cu}_{0.03}$ at depths of 1, 10, and 50 μm .

Depth [μm]	Co [%]	Fe [%]	Mg [%]	Si [%]	Ni [%]	Cr [%]	P [%]	S [%]
1	0.000445	0.001774	0.001038	0.005482	0.002384	0.001593	0.001818	0.00357
10	0.0000502	0.000721	0.00115	0.001377	0.001102	0.001159	0.002745	0.001454
50	0.000361	0.000425	0.001412	0.000691	0.001425	0.000769	0.001892	0.001387

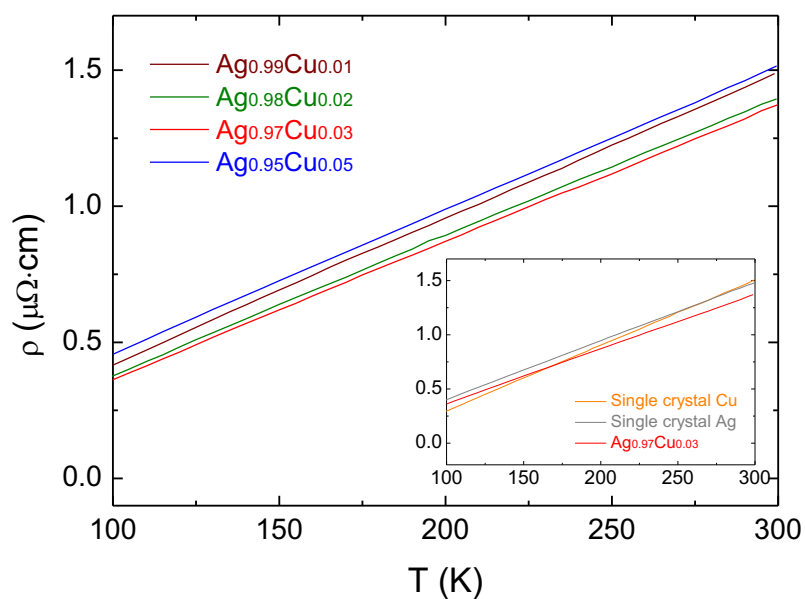


Figure S3. Temperature dependence of the electrical resistivity of the mixed crystals in the temperature range of 100–300 K. The inset shows the temperature dependence of the resistivity of $\text{Ag}_{0.97}\text{Cu}_{0.03}$, as compared with that of pure single-crystal Ag.

Figure S3 shows the electrical resistivity of the crystals in the temperature range of 100–300 K. The mixed crystals showed a drop in the resistivity with increasing Cu content in the range of 1–3 mol% and a subsequent rise for the 5 mol% sample. The quality of the mixed crystal $\text{Ag}_{0.95}\text{Cu}_{0.05}$ was not worse than that of the other samples. The temperature dependence of the resistivity was reproducible. As shown in the inset, the mixed crystal $\text{Ag}_{0.97}\text{Cu}_{0.03}$ had a lower resistivity than that of the pure single-crystal Ag.

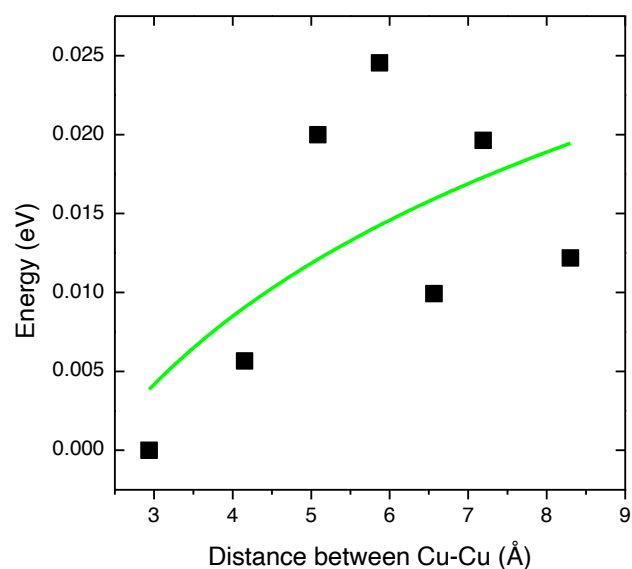


Figure S4. Total energy of the Cu-doped Ag system as a function of the distance between two Cu atoms. The value of the total energy for the Cu–Cu dimer system was set to zero.

Figure S4 shows the total energy of the Cu-doped Ag system as a function of the distance between two Cu atoms. The ionic positions were relaxed within the constant volume for the total energy calculation. The total energy of the Cu–Cu dimer system, which has the shortest distance, was the lowest value and was set to zero. A solid line from $E = k(\text{distance})^a$, where k and a are fitting parameters, is plotted for guidance.

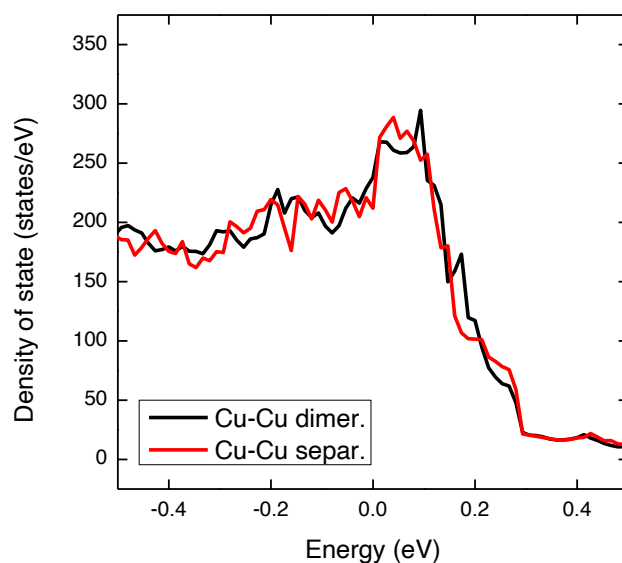


Figure S5. Density of states for the Cu–Cu dimerized and separated systems. The Fermi level of each system was set to zero.

Figure S5 shows the density of states (DOS) of the Cu–Cu dimerized and separated systems. The difference near the Fermi level is clearly shown. Note that the density of states ranging from about -0.2 to 0.2 eV contributes to carrier transport at room temperature. The difference of the DOS between the two systems, i.e., $\text{DOS}[\text{Cu–Cu dimer.}] - \text{DOS}[\text{Cu–Cu separ.}]$, was integrated in the range from -0.2 to 0.2 eV and showed a positive value of ca. 1.7 states, which is attributed to the smaller value of the electrical resistivity of the Cu–Cu dimerized system compared with that of the Cu–Cu separated system.